International Journal of Medical Microbiology 320 (2025) 151661

Contents lists available at ScienceDirect

International Journal of Medical Microbiology

journal homepage: www.elsevier.com/locate/ijmm

Helicobacter pylori CagT4SS proteins CagN and CagM bind DNA and CagN is involved in heptose-independent pro-inflammatory substrate translocation by the T4SS

Simon H. Bats [a], Felix Metz [a], Johanna Beilmann [a], Christine Josenhans [a,b,*]

[a] Max von Pettenkofer Institute, Chair for Medical Microbiology and Hygiene, LMU Munich, Pettenkoferstrasse 9a, München 80336, Germany
[b] DZIF partner site Munich, Germany

ARTICLE INFO

Keywords:
Type four secretion system
Bacterial membrane transport
Helicobacter pylori
DNA
Binding protein
Innate immunity
Pathogen-host interaction

ABSTRACT

The Cag type 4 secretion system (CagT4SS) of *Helicobacter pylori* is encoded on the *cag* pathogenicity island (*cag*PAI) that is present in about 60 % of all strains. It translocates the effector protein CagA, DNA and small bacterial metabolites into human cells. The transport mechanisms of these substrates are not clear and may involve Cag proteins still in search of a function. CagN is a partially surface-exposed CagT4SS protein with a poorly described function. The *cagN* gene is present in all *cag*PAI-positive strains and thus likely to be of importance and indispensable for the functionality of the T4SS. CagM is an essential structural component located within the outer membrane core complex of the CagT4SS in the bacterial outer membrane. CagM has a close genomic association and interacts directly with CagN. In this study, we addressed two questions on the basis of prior findings of T4SS-dependent DNA transport and TLR9 activation by *H. pylori* in host cells. First, we analyzed the role of CagN and CagM in the binding of the presumed CagT4SS substrate DNA. Second, we attempted to elucidate a presumed functional role of CagN in heptose-independent T4SS substrate translocation which may lead to pro-inflammatory activation in human cells. Using electrophoretic mobility shift assays (EMSA) and thermal shift assays (TSA), we found that both CagM and CagN interact with dsDNA. They can also act as nucleases and cleave DNA. Since the transport of substrates through the CagT4SS is likely ATP-driven, we also determined whether CagM and CagN can process ATP, which tested positive for both proteins. Co-incubating *H. pylori* with human TIFA-k/o cells, which no longer respond to the bacterial translocated effector heptose, but can still be activated by DNA, we established a phenotype of loss of heptose-independent pro-inflammatory activity with *H. pylori cagN* mutants that could be reversed by complementation. Our results propose an important role for CagN and CagM to bind DNA which might impact or be involved in the transport of substrates such as DNA, through the CagT4SS.

1. Introduction

Type four secretion systems (T4SS) of Gram-negative bacteria are very heterogeneous in nature and can transport various substrates. They contribute to DNA transport between bacteria by conjugation or natural competence (Fischer et al., 2020; Ryan et al., 2023a; Waksman, 2025), translocate DNA into plant cells in the case of *Agrobacterium tumefaciens* (Li and Christie, 2018) and can also transport other molecules such as metabolites and proteins (Gomez-Valero et al., 2019; Hilbi et al., 2017; Stein et al., 2017; Costa et al., 2021). An interesting variant are the T4SS type 2b and type 2c systems which appear to transport predominantly proteins into human host cells to confer virulence properties or colonization benefit, e.g. by the targeted secretion systems of the pathogenic bacteria *Legionella pneumophila* and *Helicobacter pylori* (Censini et al., 1996a; Hilbi et al., 2017; Tan et al., 2011). The latter two systems which are more complex in composition have been structurally well characterized in recent times (reviewed in Sheedlo et al., 2022), but are still functionally underexplored with respect to transport functions and possible transport substrates other than proteins.

Highly virulent strains of *H. pylori* contain a 32 kB genetic element, the *cag* pathogenicity island (*cag*PAI) (Censini et al., 1996; Odenbreit et al., 2000; Stein et al., 2000; Olbermann et al., 2010). This genetic

* Corresponding author at: Max von Pettenkofer Institute, Chair for Medical Microbiology and Hygiene, LMU Munich, Pettenkoferstrasse 9a, München 80336, Germany.
E-mail address: josenhans@mvp.lmu.de (C. Josenhans).

https://doi.org/10.1016/j.ijmm.2025.151661
Received 17 April 2025; Received in revised form 6 June 2025; Accepted 23 June 2025
Available online 23 June 2025

island codes for the Cag Type 4 Secretion System (CagT4SS), which spans the inner and outer membranes of the bacteria and transports the protein effector CagA (Odenbreit et al., 2000), small metabolites (Stein et al., 2017; Zimmermann et al., 2017; Pfannkuch et al., 2019) and DNA (Varga et al., 2016), among others, into human cells. In addition to the 12 proteins that are highly homologous to the VirB/D system of *A. tumefaciens,* the CagT4SS codes for additional components of unknown functions. CagN and CagM are two of these *H. pylori*-specific accessory proteins with poorly described functions. CagM and CagN interact with each other, and CagM also forms homotypic oligomers, while CagN seems to be mostly monomeric in solution (Bats et al., 2018). CagM is part of the inner core of the membrane-spanning structure of the CagT4SS in the outer membrane, can bind to several proteins of the CagT4SS core complex (Busler et al., 2006; Sheedlo et al., 2020), and is required to build up the CagT4SS system (Sheedlo et al., 2020; Roberts et al., 2024). We and others have shown that CagN is surface-exposed in *H. pylori* (Bourzac et al., 2006; Bats et al., 2018). Their proposed transport pathway to the outer membrane complex (OMC) of the T4SS or to the bacterial surface is likely to be dependent on the CagT4SS (Bats et al., 2018). Functions of CagN in the system are not evident so far.

CagT4SS-dependent bacterial secretion of DNA, and DNA transport into target cells, followed by activation of the cellular pattern recognition receptor (PRR) TLR9, which binds double-stranded (ds) DNA, was only recently reported (Varga et al., 2016), however the mechanisms of the proposed DNA transport remain so far unknown. We surmised that the transport of DNA needs T4SS accessory proteins that provide energy for trans-T4SS transport and helper proteins that may be involved in substrate, e.g. DNA, transport towards the human cell.

T4SS possess inner membrane-associated protein components with ATPase function, namely the VirB4, VirD4 and VirB11 homologs. The energy they provide is thought to be essential for inner membrane transport of various export substrates through the T4SS (Atmakuri et al., 2004; Christie, 1997; Andrzejewska et al., 2006; Peña et al., 2012; Hu et al., 2019). However, how energy provisioning works for transport through the rest of the membrane passage through the T4SS, including the outer membrane complex, is unclear. Other proteins might provide energy for transport, for instance by ATP binding and cleavage. Protein nucleotide binding domains, which may generally allow the binding of ATP and other nucleoside triphosphates as well as DNA, consist of three characteristic and mostly conserved motifs (Walker A, B, and C motifs) (Walker et al., 1982; Qin et al., 2008), which have been identified in the Cag inner membrane ATPases, but so far not in other proteins of the CagT4SS. The transport of DNA to the outer surface of the bacterial secretion system would be envisaged to likely involve interactions with transporter proteins and with one or more proteins of the outer membrane core complex ($OMCC_{Cag}$) of the T4SS to thread the DNA through the system.

On the basis of prior reports of activation of the dsDNA PRR TLR9 by the *H. pylori* CagT4SS, which requires DNA translocation through the T4SS, in this study we explored the hypothesis that CagN (and CagM) may possess accessory protein functions that could be useful to transport secretion system substrates, either by directly binding substrates, or by providing energy for such transport processes. We therefore analyzed DNA binding for the proposed transport accessory protein CagN, and in addition, to the OMCC structural core protein CagM, which is closely linked to CagN by co-expression, exploring the hypothesis that both proteins may be involved in the transport process of non-protein substrates.

We also analyzed both proteins for potential ATP-binding sites and found possible Walker B and C motif sequences in CagM. We found that both Cag proteins can bind DNA and cleave ATP. Moreover, we lay functional groundwork to suggest that CagM and CagN may be involved in non-heptose substrate transport through the CagT4SS towards the host cell.

2. Methods

2.1. Cloning and protein expression and purification in Escherichia coli

The cloning and purification procedures of $CagN^{WT}$, $CagN^{C4A}$, $CagN^{\Delta C90}$ and $CagM^{WT}$ were described previously in detail (Bats et al., 2018). Briefly, *cagN* variants and $cagM^{WT}$ were cloned into pET28a(+) (Merck Millipore Novagen, Burlington, Massachusetts, USA) behind the plasmid encoded N-terminal 6xHIS-tag with the RE enzymes *Bam*H1 and Not1 (NEB (primers in Table S1). A Tobacco Etch Virus nuclear-inclusion-A endopeptidase (TEV protease) cleavage site was introduced between the 6xHis-tag and the start codon of CagN, leaving a tag-free protein after cleavage. The predicted sequences of the resulting protein preparations are listed in Table S2. Plasmids were transformed into *E. coli* expression strains BL21(DE3) (Table S3) for $CagM^{WT}$ and Rosetta™(DE3) pLysS (Novagen, Merck, Germany, Table S3) for CagN variants. Protein expression was induced with 0.2 mM IPTG for 4 h at 30°C (CagN variants) or 0.1 mM IPTG for 4 h at 28°C ($CagM^{WT}$). Cells were harvested, the pellets resuspended in Tris-based buffers and lysed by sonication. CagN was purified from the soluble lysate fraction, CagM was extracted with urea from the insoluble lysate fraction for purification. All purification steps were performed on an Aekta Prime plus instrument (Cytiva, Freiburg, Germany) at room-temperature with buffers cooled on ice. Proteins were purified in a first step on Protino Ni-NTA columns (Macherey-Nagel, Düren, Germany). For all purifications, a high-salt wash step with 1 M NaCl in buffer was performed to remove DNA remnants and other contaminants. CagN was additionally tag-cleaved with self-purified TEV protease and reloaded on Protino Ni-NTA columns to remove protease and uncleaved protein. Highest purity was obtained after a subsequent ion-exchange chromatography purification to remove any remnants of bound nucleotides or DNA (CagN) (three-step purification). Quality and purity of preparations were verified using SDS-PAGE, Western blot, and biophysical methods (Bats et al., 2018). If required, CagN and CagM proteins were analyzed in Western blots and detected with our custom-generated rabbit antisera (Bats et al., 2018).

2.2. Site-directed mutagenesis of CagN

Point mutations of *cagN* to $cagN^{KFSR}$ were introduced with the QuickChange site-directed mutagenesis kit (Stratagene, La Jolla, USA) and the primers $HP0538^{KSFR}$_fw + $HP0538^{KSFR}$_rv (Table S1), using the pET28a-$cagN^{WT}$ expression plasmid (Bats et al., 2018), according to the manufacturer's protocol. The $CagN^{KFSR}$ mutant was purified according to the three-step protocol of $CagN^{WT}$. We generated the point mutations in pET28a-TEV^{CS}-$CagN^{[25-306]}$ for expression in *E. coli* (Bats et al., 2018) and pUC18-*rdx*::-p^{CagMN}-$CagN^{[1-306]}$ (complementation construct pCJ1600, described in (Bats et al., 2018) for expression in *H. pylori*). Primers for mutagenesis are listed in Table S1.

2.3. Generating mutants and complementation strains in H. pylori

Isogenic insertion-inactivation mutants in the *cagM* and *cagN* genes of *H. pylori* (strain N6) were described previously (Bats et al., 2018). Genes cloned into *Escherichia coli* plasmids pUC18 or pUC19 (suicide plasmids in *H. pylori*) were disrupted by partial gene deletion and insertion of a kanamycin resistance cassette (*aphA3′-III*) from *Campylobacter coli* (Labigne-Roussel et al., 1988), followed by allelic exchange with the wild type gene copy after homologous recombination in *H. pylori*. Plasmid constructs were first generated in *E. coli* (cloning primers listed in Table S1). The resistance cassettes were inserted in the same orientation as the target gene and constructs verified by PCR and partial sequencing. Complementation strains (in *H. pylori* strain N6, *cagN* mutant) were generated by reintroducing $cagN^{wt}$ (cloned from strain HP87P7; (Behrens et al., 2013)) downstream of the *cagM* promotor (strain HP87P7) into the *H. pylori rdxA* gene, accompanied by a

chloramphenicol resistance gene cassette (cm), as previously described, on the basis of plasmid pCJ542 (Behrens et al., 2013), yielding plasmid pCJ1600. *H. pylori* were grown on Columbia blood agar plates with 5 % horse blood (Oxoid blood agar base no. 2, Thermo Fisher Scientific, Waltham, Massachusetts, USA), supplemented with the antibiotics amphotericin B (4 mg/liter), polymyxin B (3 mg/liter), trimethoprim (5 mg/liter) and vancomycin (10 mg/liter), at 37°C under microaerobic conditions (10 % CO_2, 5 % O_2, 8.5 % N_2). Allelic exchange mutants were selected on agar containing additional kanamycin (20 mg/liter). Plasmid constructs and insertions into the *H. pylori* chromosome were verified by DNA isolation, PCR, and Sanger sequencing (primers see Table S1). All *H. pylori* strains used in this study are listed in Table S3. Expression or lack of expression of CagN and CagM proteins in the mutants and complementants was detected in Western blots with our specific custom rabbit antisera (Bats et al., 2018).

2.4. Generation of dsDNA fragments for cleavage assays and EMSA

282 base pair (bp) long fragments (F-GC^{29}, F-GC^{39}, and F-GC^{45} as well as GC^{29}, GC^{39}, and GC^{45}, Table S4) were generated by PCR with the oligonucleotides listed in Suppl. Table S1 and subsequent PCR purification (NucleoSpin Gel and PCR Clean-up Mini kit, Macherey-Nagel, Düren, Germany) and eluted in EB buffer. DNA concentrations were determined in a NanoDrop instrument (Thermo Fisher Scientific, Waltham, Massachusetts, USA). All DNA samples exhibited a single band on 2 % agarose gels. The superscripted number in the DNA fragments' names indicates the GC content for each fragment. Long DNA fragments with an "F"-prefix contain an additional IRDye-700 label at one 5' end (Table S4) (primers see Suppl. Table S1). 2 pmol of each primer were heated to 95°C for 5 min and slowly cooled down to 25°C, for annealing and forming double strands, with a cooling rate of 1°C per 10 s, freshly before each experiment. Both fluorescent labels DY-682 and IRDye-700 have similar absorption (685 nm versus 690 nm) and emission (705 nm versus 709 nm) spectra and can replace each other [https://eurofinsgenomics.eu/media/144266/application-note_licor.pdf].

The sequence of GC^{45} is an artificial PCR-amplified sequence that contains the multiple cloning site of the pHel2 plasmid (Heuermann and Haas, 1998). GC^{29} and GC^{39} contain segments of genes in the *H. pylori* genome. They encode parts of the class I SAM-dependent methyltransferase – adenine-specific DNA methyltransferase (VspI/ HP0478, GC^{29}) and vacuolating cytotoxin domain-containing protein (VacA2, HP0610, GC^{39}), respectively.

2.5. Electrophoretic mobility shift assay (EMSA)

Previously published EMSA protocols (Chen et al., 2011; Hellman and Fried, 2007) were optimized for CagN and CagM. 0.5 pmol purified DNA fragments were incubated with variable amounts of protein of interest (POI) on ice for 30 min with 1.25 µl of 4x assay buffer (60 mM Tris/HCl (pH 8.0), 60 % Glycerol, 600 µM EDTA (pH 8.0), 300 mM KCl, 7 mM DTT, 30 mM $MgCl_2$, 5 % Tween-20 and 0.004 % Bromophenol blue) in a total reaction volume of 5 µl. For experiments with CagN variants, the reaction mixture was, subsequently to the binding incubation, cross-linked at 40 mJ in a CL-568 UV-cross linker (Techne).

Non-denaturing acrylamide gels, composed of a degassed mixture of 6.55 ml H_2O, 0.4 ml 10x TGE, 0.9 ml 40 % acrylamide stock (Acrylamide/Bis-solution, 29:1), 200 µl glycerol (50 % vol/vol), 60 µl 10 % APS and 6 µl TEMED were poured. Gels were pre-run (2 h at 10 mA in a cold room) to enhance the gel quality. Samples were loaded and the gels run at 7 mA on ice for 60 min. Gels with fluorescently labeled DNA fragments were scanned with the IR_{short} filter in a Typhoon scanner (Cytiva, Freiburg, Germany) at 25 µm resolution to visualize labeled DNA. We performed control experiments with BSA (Pierce™ BCA Protein Assay Kit, Thermo Fisher Scientific, Waltham, Massachusetts, USA).

2.6. Thermal shift assays (TSA)

TSA were performed with highly pure $CagM^{WT}$ and CagN variants in transparent 96 well plates (AB-0700, Thermo Fisher Scientific, Waltham, Massachusetts, USA) with an adapted protocol (Kranz and Schalk-Hihi, 2011) in a Biorad CFX96 (Bio-Rad, Hercules, USA) or ABI 7000 (ABI, Applied Biosystems Inc.) thermocycler. 6 µg of $CagM^{WT}$ or 4 µg of CagN protein were mixed with variable amounts of ligands (Na^{2+}-ATP (Sigma-Aldrich) and DNA fragments) as indicated, 5x (final dilution) SYPRO Orange (5000x Stock-Solution, #S5692–50, Sigma-Aldrich) buffered with 50 mM Tris/HCl pH 7.5; 150 mM NaCl; 1 mM DTT (CagM) or 50 mM MES pH 6.0; 200 mM $CaCl_2$, 1 mM DTT (CagN) in 25 µl reactions. Plates and protein solutions were kept on ice during all pipetting steps. The sample temperature was increased at a ramp rate of 1 °C/min from 5°C to 95°C, and fluorescence was measured every 0.5°C in the thermocycler in FRET mode. Curves were evaluated and displayed with the web applications TSA Craft (Lee et al., 2019) or JTSA/MTSA (Schulz et al., 2013). Determination of K_D values was performed with GraphPad (GraphPad Software, San Diego, USA).

2.7. DNA cleavage assays

DNA cleavage assays were performed to test potential nuclease activities of CagM, CagN and BSA (control protein) and adapted from (Burkovics et al., 2009) and Thermo Fisher Tech Bulletin #171 http://www.lifetechnologies.com/de/de/home/references/ambion-tech-support/rna-isolation/general-articles/gel-purification-of-probes-for-nuclease-protection-assays.html). 0.5 pmol of appropriate double-stranded DNA (see above) was incubated with variable amounts of the highly-pure POI in 40 mM Tris/HCl (pH 7.5); 8 mM $MgCl_2$; 1 mM DTT; 150 mM NaCl in a reaction volume of 7 µl for 2 h at 37°C. 14 µl of a 20 mM EDTA, 95 % formamide, 0.25 % bromophenol blue solution were added. Formamide enables the DNA denaturing. 15 µl of the samples were loaded on DNA-denaturing 12.5 % acrylamide / 8 M urea gels (3.84 g urea; 0.8 ml 10X TBE; 2.5 ml 40 % acrylamide (acrylamide: bis acrylamide = 29:1); 1.3 ml H_2O; 80 µl 10 % APS; 3.5 µl TEMED). Gels were run for 10 min at 100 V and then 30–45 min at 200 V in 1x TBE buffer. Gels were scanned with the IR_{short} filter in a Typhoon scanner (Cytiva) to visualize labeled DNA. dsDNA fragments were primer-labeled on one strand with IRDye700 or DY-682 for detection (see above). BSA control protein with dsDNA, or dsDNA incubated without protein did not lead to a detectable fragmentation of the DNA templates.

2.8. ATP quantification test

To test purified protein preparations (CagN, CagM) for potential ATP contamination, we quantitated the absolute ATP amounts in the preparations using the ATP-Glo™ Bioluminometric Cell Viability Assay (Biotium, Fremont, USA). 5 µg of purified protein of interest were diluted in water to a total volume of 100 µl. ATP standard dilutions and the ATP-Glo Detection Cocktail were prepared according to the manufacturer's instructions. 100 µl ATP-Glo Detection Cocktail were added to each sample and ATP standard. Luminescence was subsequently measured (as arbitrary units [AU]) in white flat-bottom plates (Greiner) at a Victor Nivo multi-well reader (PerkinElmer, Waltham, Massachusetts, USA) with 1 s integration time and unfiltered luminescence. A linear fit was applied to the standard values to quantify the ATP content of samples.

2.9. ATPase assay

In order to detect ATP cleavage by purified proteins, we also used the ATP-Glo Bioluminometric Assay (Biotium; see above). Variable amounts of $CagM^{WT}$ and $CagN^{WT}$ were co-incubated with 10 pmol ATP and 2.5 µl 10x Buffer A (500 mM Tris/HCl pH 7.5; 150 mM NaCl; 10 mM DTT) for

2 h at 37°C in a total reaction volume of 25 µl. Afterwards, 75 µl H_2O was added. Luminescence was measured after the addition of 100 µl ATP-Glo Detection Cocktail as described in the ATP quantification test instructions by the manufacturer. The measured concentrations of ATP (as arbitrary units [AU]) were compared to a standard curve with 10, 5, 2, 0.5, and 0 pmol ATP and sample values [pmol] were accordingly calculated (Table 1).

2.10. Cultivation of human cells and co-incubation experiments with live bacteria

AGS-TIFA$^{k/o}$ (Stein et al., 2017) cells were cultivated in RPMI 1640 medium (supplemented with 20 mM Hepes, GlutaMAX stable amino acids (Gibco, Thermo Fisher Scientific), and 10 % FCS (PromoCell, Germany). HEK-TIFA$^{k/o}$ cells (Stein et al., 2017) and HEK-NF-κB_luc cells (Hauke et al., 2023) were cultivated in DMEM (buffered with 20 mM Hepes and Glutamax (Gibco, Thermo Fisher Scientific, USA) and 10 % FCS, whereby the latter cell line was supplemented with 50 µg/µl hygromycin B (Invivogen, USA). All cell lines were frequently passaged and routinely grown at 37°C and 5 % CO_2. Co-cultivation with *H. pylori* strains was performed in 24- or 96-well plates in the respective media without antibiotics. In preparation, cells were cultured after seeding overnight, up to 60–80 % confluency, before adding the bacteria. Bacterial OD_{600} of freshly grown bacteria (20–24 h on fresh plates) was measured and adjusted in cell culture medium and bacteria were added to the cells at different MOIs (indicated in figure legends). The co-incubations were carried out further for 3 h with HEK-luc cells and for 20 h with AGS-TIFA and HEK-TIFA cells. Cell transfection of HEK--TIFA$^{k/o}$ cells with plasmids was performed in 24-well plates using Lipofectamine 2000 (Invitrogen) according to the manufacturer's instructions, with 200 ng of plasmid per well. Transfected cells were used for activation assays at 24 h post-transfection. Supernatants of co-cultures were harvested and IL-8 ELISA was performed at suitable dilutions according to the manufacturer's protocol (BD OptEIA Human IL-8 ELISA Set, San Diego, USA). For HEK-luc cells, luciferase activity was detected in three or four independent biological replicates using SteadyGlo reagents (Promega) and measured in a multi-well plate reader (Victor Nivo) in white plates. Innate immune ligands (γ-D-glutamyl-meso-diaminopimelic acid - ieDAP [NOD1 ligand, Invivogen], *E. coli* ultrapure LPS [TLR4 ligand, List Biologicals]; PamCysS4K lipopeptide [TLR2 agonist, Invivogen], L-ADP heptose [ALPK1 agonist, Invivogen], and muramyl-dipeptide MDP [NOD2 ligand, Invivogen]) were added in parallel to the cells at appropriate concentrations to test for cell activation (figure legends).

2.11. AlphaFold 3

AlphaFold 3 (Abramson et al., 2024) was used as a standard modelling tool for protein monomers. The amino acid sequences of CagN and CagM from *H. pylori* strain 26695 were submitted to the AlphaFold 3 server (https://alphafoldserver.com/) as a "Protein" entity, either as a single or double copy. For the dsDNA binding, two complementary strands of 100 bp with an approximate GC content of 39 % corresponding to the average core genome GC content of *H. pylori* 26695 were added as "DNA" entity. dsDNA binding predictions were run in multimer mode with and without ATP as a "Ligand" entity and 10 Mg^{2+} as "Ion" entity. The different models obtained as output were manually evaluated taking into account their per-residue predicted Local Distance Difference Test (pLDDT) scores. Visual representation as well as display of interaction interfaces was performed with UCSF ChimeraX (Meng et al., 2023).

3. Results

3.1. CagN and CagM both bind linear dsDNA fragments

We performed EMSA experiments to analyze the binding of CagM^{WT} (Fig. 1) and CagN^{WT} (Fig. 2) to dsDNA fragments. We initially used F-GC^{39} fragment (of approximately 300 bp length) with the same GC content of 39 % as the average GC content of the *H. pylori* genome (e.g. determined for strain 26695) (Alm et al., 1999). Both proteins were able to bind the tested DNA fragment which seemed to be non-specific (Fig. 1 A, Fig. 2 A). We obtained a concentration-dependent shift towards the upper band (DNA-protein complex), reducing the lower band (dsDNA only). The binding of CagM^{WT} to dsDNA had an approximately five-fold higher affinity than that of CagN^{WT}, extrapolated from the respective initial shifting concentrations (Fig. 1 A, Fig. 2 A). In our first assays, it proved challenging to reproducibly detect the up-shifted CagN^{WT} - dsDNA band in EMSA gels (own unpublished results). This technical issue could be strongly improved after we performed a UV-crosslinking step after the binding incubation (Methods), before the EMSA gel run, as described in the methods section.

The detected interaction of the two proteins with DNA had an estimated low- to medium- affinity and we speculated it might be different for differently composed DNA fragments. To address the question of binding specificity further, we analyzed two additional DNA fragments of the same length but different sequence and GC contents. Interactions of CagM^{WT} and CagN^{WT} with F-GC^{45} (Fig. 1 B, Fig. 2 B) as well as with F-GC^{29} (Fig. 1 C, Fig. 2 C) were also detectable in these experiments. The protein-DNA interaction did not seem to be clearly dependent on the GC content of the DNA or to require a specific sequence. The binding affinity

Table 1
ATPase activities of CagN and CagM (IC_{50}).

Sample/Protein	Raw [AU]	Corrected [AU]	ATP [pmol]	Original [%]	Reduction [%]
1 µg CagN	292896	290781	9.323	93.23	6.77
5 µg CagN	204622	202507	6.508	65.08	34.92
15 µg CagN	138606	136491	4.402	44.02	55.98
1 µg CagM	114739	112624	3.64	36.40	63.60
5 µg CagM	4690	257	0.130	1.30	98.70
10 µg CagM	3566	1451	0.094	0.94	99.06
Standard concentrations					
10 pmol ATP	322829	320714	10.278		
5 pmol ATP	143525	141410	4.559		
2 pmol ATP	34298	52183	1.712		
0.5 pmol ATP	14747	12632	0.451		
Blank	2115	0			

Table 1: 10 pmol of ATP were coincubated with different amounts of CagN^{WT} and CagM^{WT} for 2 h at 37°C. The amount of ATP decreases in the CagN and CagM samples. The decrease is concentration dependent. The ATPase activity of CagN is rather low, after two hours with 5 µg protein the amount is reduced by about one third. The activity of CagM is more than one order of magnitude higher. Abbreviations: Raw: Measured raw values (luminescence in arbitrary units [AU]); Corrected: blank values were subtracted from raw values; Original: Remaining percentage of ATP compared to initial amount in [%] (original amount is 10 pmol).

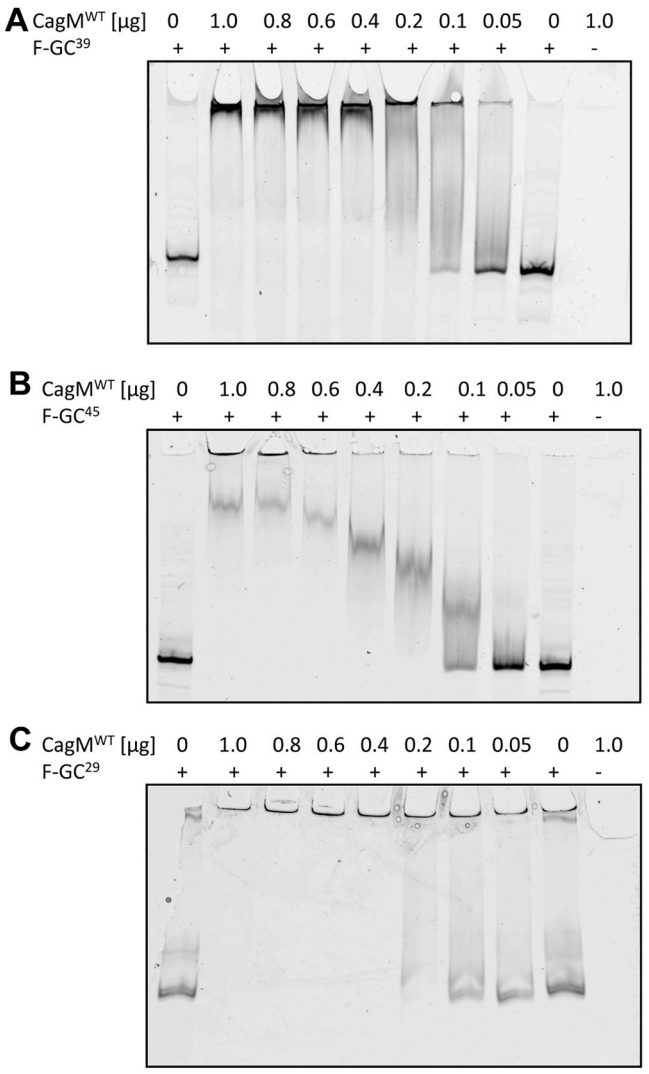

Fig. 1. CagM binds dsDNA of different GC content as assessed by EMSA. Purified recombinant CagM protein shows a concentration-dependent shift in EMSA when co-incubated with double-stranded test DNA. 0.5 pmol fluorescently labeled dsDNA F-GC^{39} (A), F-GC^{45} (B) and F-GC^{29} (C) were co-incubated with CagM in different amounts, between 0.05 and 1 µg. Concentration-dependent band shifts were detected for all three DNA fragments, with similar shifts at 0.2 µg CagM.

of CagN^{WT} appeared to be slightly lower for the latter two fragments, in particular for the low GC content fragment F-GC^{29} (Fig. 1 C, Fig. 2 C). BSA was tested as a negative control and did not shift dsDNA (Fig. 2 D).

3.2. Testing potential dsDNA binding regions of CagN by deletion and site-directed mutagenesis

Since there are no high-resolution structures of CagM and CagN available, it is challenging to detect residues or patches in the tertiary structure that could be important for the protein-DNA interaction. We first performed a computational analysis with the software PredictProtein (Bernhofer et al., 2021) to search for patterns within full-length CagN that are predicted to be surface-exposed and might be involved in DNA binding. Four possible motifs/patches with lengths from three to eight amino acids were detected (Fig. 3 A). We did not prioritize three of those patterns as primary targets for binding, because they were either located in the potential leader peptide (amino acids 1–24) which was not included in the tested recombinantly purified CagN preparations (patch 1: Y^{19}GGLN^{23}) nor in the last 90 amino acids (cleaved off in the mature CagN protein in *H. pylori*) (Bourzac et al., 2006), (motifs 3: S^{230}NNRTF^{235}, 4: K^{286}SE^{288}, Fig. 3 A). Motif 2 (N^{213}KFSRQHL^{220}) is the only motif that is predicted to remain in the mature cleaved N-terminal domain of the CagN protein. It is located directly at the natural cleavage site (after amino acid S216) (Bourzac et al., 2006) and also predicted to be predominantly surface-exposed and flexible and therefore presents a plausible patch for substrate binding (Fig. 3 A). In order to experimentally test potential binding sites, we performed EMSA assays with recombinantly purified CagN variants; first for one variant, in which all four cysteine residues are point-mutated to alanine, which might affect the stability of the tertiary structure (CagN^{C4A}, Fig. 3 B, (Bats et al., 2018)), and second, in a mutated protein that is C-terminally truncated, lacking the last 90 amino acids after the natural cleavage site (CagN$^{\Delta C90}$, Fig. 3 C, (Bats et al., 2018)). Both mutants still retained the DNA binding and shifting affinity in EMSA (Fig. 3 B, C). The last 90 amino acids and the cysteine residues are therefore likely not essential for the dsDNA interaction, but the ΔC90 variant seemed to exhibit reduced DNA binding. Lastly, we cloned, recombinantly expressed and purified a CagN mutant named CagN^{KFSR}, in which the putative binding motif aa^{213}KFSRQHL^{220} close to the proteolytic site (patch 2 in overview Fig. 3 A) was point-mutated to aa^{213}AAAAQHL^{220}. The CagN-DNA interaction was still detectable with this mutant in EMSA experiments (Fig. 3 D), but binding also seemed to be weaker than for wild type CagN.

To complement our binding experiments, we performed, under different buffer conditions (Methods), DNA cleavage assays to test for potential nuclease activities of CagN and CagM on dsDNA (Fig. S1). A time-dependent nuclease activity of CagN^{WT} was detected on F-GC^{39} dsDNA (Fig. S1 A). CagM^{WT} also showed a nuclease activity with a different fragmentation pattern (Fig. S1 B, C). While CagN$^{\Delta C90}$ and CagN^{KFSR} variants retained nuclease activity, it was weaker than for the wild type protein (Fig. S1 D, S1 E).

3.3. Biophysical experiments confirm the interactions of CagN and CagM with DNA

In order to confirm the interactions of CagM and CagN with DNA using a second method, we performed thermal shift assays (TSA) for CagM^{WT} and variants of CagN. CagM^{WT} showed a reproducible, concentration-dependent temperature shift (shift of T_m) in TSA with dsDNA fragments GC^{39} (Fig. 4 A to G), compared to CagM without DNA. Buffer (Fig. 4 H) or DNA alone (Fig. 4 I) yielded a very low background. We evaluated the curves with the web applications MTSA/JTSA (Schulz et al., 2013) and TSA Craft (Lee et al., 2019). CagM TSA curves without any added potential binding partners were reproducible and easily fitted. We determined a T_m of 47.8°C ± 0.1°C under optimized assay conditions for CagM^{WT} alone, without DNA or other potential binding partners (Fig. 4 A). Together with dsDNA, a ΔT_m of more than 2°C was derived by TSA between DNA concentrations of 1 nM and 200 nM, from curve analysis with MTSA (Schulz et al., 2013) and TSA Craft (Lee et al., 2019) (Fig. 4 G). AlphaFold 3 (AlphaFold multimer) (Abramson et al., 2024)(Methods) modelled a dsDNA binding for a monomer of CagM with 10-fold Mg^{2+} and one molecule of ATP (Fig. S2), indicating multiple amino acid patches, containing positively charged amino acids, along the whole length of the protein to be potentially involved in DNA binding (Fig. S2 for details).

CagN is predicted to be an elongated, alpha-helical protein likely containing several intrinsically disordered regions which may render the isolated protein structurally instable (Bats et al., 2018), much less structurally stable than CagM. Despite extensive testing of CagN^{WT} and CagN$^{\Delta C90}$ alone with various buffers and protein preparations, we did not obtain TSA curves of sufficient quality or reproducibility to derive a stable T_m or a concentration-dependent T_m shift with dsDNA (data not shown). We therefore tested the CagN – DNA interaction aided by Surface Plasmon Resonance in Biacore (Fig. S3). In addition to dsDNA binding by EMSA, we experimentally detected a weak interaction with

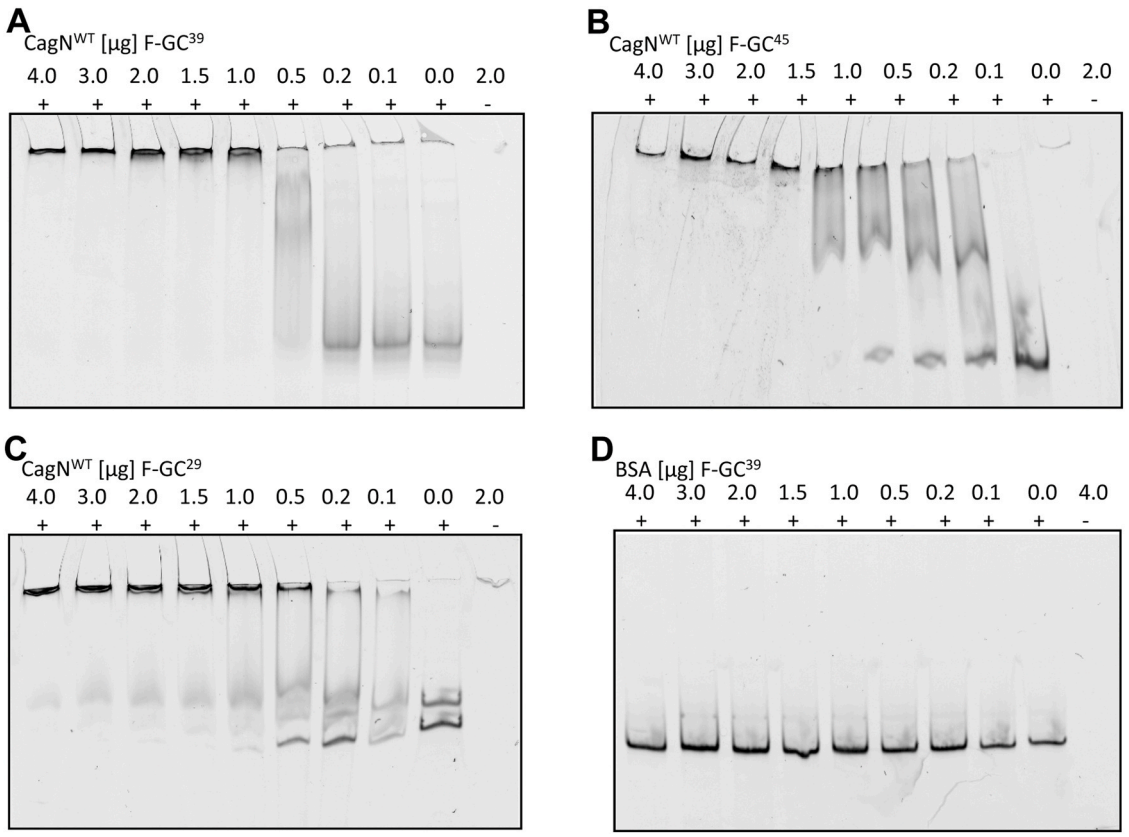

Fig. 2. CagN binds dsDNA of different GC content in EMSA. Purified recombinant CagN causes a concentration-dependent shift with dsDNA in EMSA. 0.5 pmol fluorescently labeled dsDNA were coincubated with CagN in different concentrations. 0.1–4 µg of $CagN^{WT}$ were coincubated with $F\text{-}GC^{39}$ (A), $F\text{-}GC^{45}$ (B) and $F\text{-}GC^{29}$ (C). As a control, we analyzed a commercial pure protein preparation of BSA (Pierce) for binding to $F\text{-}GC^{39}$ dsDNA (D). BSA did not interact with the tested dsDNA fragments.

dsDNA for $CagN^{WT}$ protein as analyte in different concentrations, using biotinylated $dsDNA^{GC39}$ covalently coupled to the Biacore chip, with a low K_D of approximately 25 µM (Fig. S3 B). AlphaFold 3 modeling did not suggest the binding of a CagN monomer (Bats et al., 2018) to DNA, but indeed indicated the potential of DNA binding for $CagN^{wt}$ when a CagN dimer was offered in the context of dsDNA, 10-fold Mg^{2+} and two molecules of ATP (Fig. S4), with charged amino acids proposed to interact with the DNA. The prediction of binding residues in the CagN protein primary sequence included mainly three separate amino acid patches, one of those comprising the above-mentioned KFSR patch (Fig. 3 A), close to the CagN proteolytic cleavage site.

3.4. CagM binds ATP

The transport of substrates through the CagT4SS is ATP-dependent for the inner membrane where three specific ATPases are located, as *cagE* (VirB4) ATPase mutants and mutants in the two other Cag inner membrane ATPases of *H. pylori* (Cagα, Cagβ) show deficiency in T4SS transport functions (Fischer et al., 2001; Guillemin et al., 2002; Lin et al., 2020). On the quest of a potential additional function in energizing the export process towards the outer membrane, we analyzed CagN and CagM for potential ATP binding motifs with a bioinformatics approach using the software applications NsitePred (https://biomine.cs.vcu.edu/servers/NsitePred/), TargetATPsite (Yu et al., 2013) and ATPbind (https://zhanggroup.org/ATPbind/). No motifs were detected *in silico* in CagN or CagM protein sequences with high or medium accuracy (not shown). Several nucleotide binding domains in proteins, which allow the binding of ATP and other nucleoside triphosphates as well as DNA, consist of three characteristic and highly conserved motifs. The signature Walker A motif has the consensus GxxGxGK[S/T] (x: arbitrary amino acid), the canonical Walker B motif hhhhD (h: aliphatic residue), and the Walker C motif is LSGGQ[Q/R/K]QR, as described in the introduction section. We therefore analyzed the sequences manually for the classical ATP binding motifs (Walker A, Walker B and C motif) and detected several potential motifs in CagM (Suppl. Fig. S2 A). The hydrophobic amino acid patches within CagM, VFSLD and LLVLD, have possible similarity to Walker B motifs (Suppl. Fig. S2 A). L^{298}SFAQKQK is a possible Walker C motif sequence that fits with the consensus sequence except for the two glycine residues substituted by serine and phenylalanine in CagM. Replacements of glycine residues by other hydrophobic residues have already been described in other ATP binding proteins (Kumar et al., 2010). We therefore analyzed the binding of CagM to ATP with thermal shift assays. However, we did not observe a reproducible concentration-dependent T_m shift with ATP. AlphaFold 3 (Abramson et al., 2024) prediction of CagM, as for CagN, indicated ATP binding. We speculated that lack of experimental CagM ATP binding detection might possibly be due to an ATP cleavage activity.

3.5. Assaying ATPase activities of CagM and CagN

Consequently, we addressed the question, whether CagM and probably CagN can cleave ATP in vitro. We first performed ATP quantification tests to analyze whether the purified protein preparations contain ATP after the purification. Both protein preparations did not contain detectable amounts of ATP (Suppl. Fig. S5). Next, we performed an ATPase assay to measure the ATP amounts with a possible decrease over time, during co-incubation of different amounts of $CagM^{wt}$ or $CagN^{wt}$ with 10 pmol of Na-ATP. Both proteins exhibited a significant and concentration-dependent ATPase activity (Table 1). Those activities were concentration dependent. The ATPase activity of CagM was about

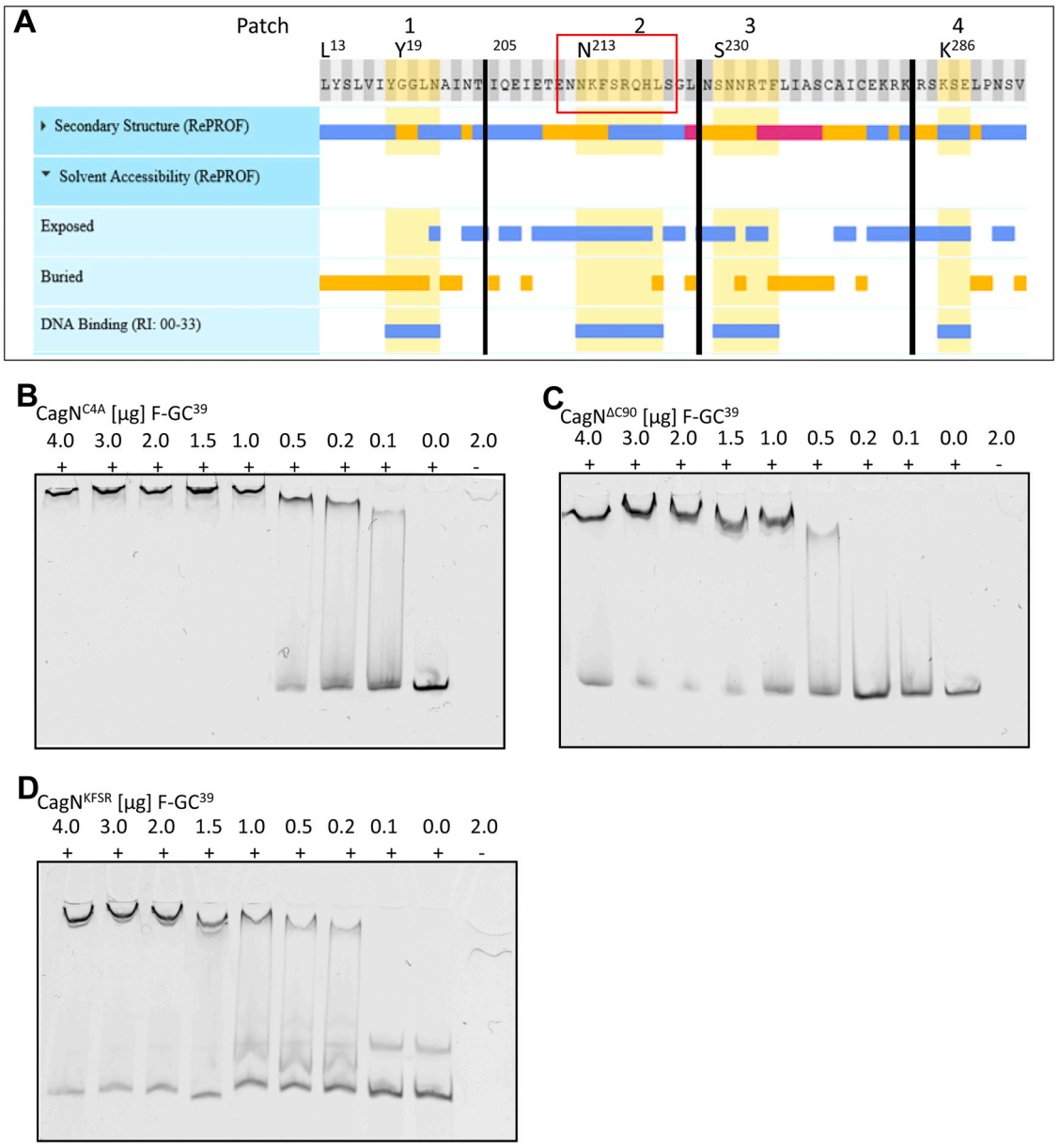

Fig. 3. CagN deletion and mutation variants in predicted DNA binding patches interact with dsDNA (EMSA). A) CagN primary sequence was analyzed for potential DNA binding motifs in the software PredictProtein. Selected CagN segments are shown as a schematic, indicated by amino acid numbers. Four linear patches within CagN (indicated in yellow) were predicted to have potential for DNA binding. They are predicted to be at least partially flexible and surface-exposed (marked in blue color). Patches numbered 1, 3 and 4 are in regions that are presumably not included in the mature CagN$^{\Delta C90}$. Patch 1 (putative leader peptide) is not included in the purified CagN$^{\Delta C90}$ protein tested in vitro. Natural CagN processing site is located after amino acid S216 in patch 2 (Bourzac et al., 2006). B) to D) Variants of CagN with deletions and mutations were tested for dsDNA interaction (GC^{39} fragment) using EMSA. EMSA was performed similar to Fig. 1, using fluorescently labelled dsDNA fragment F-GC^{39}: CagN^{C4A} (B); CagN$^{\Delta C90}$, C-terminal deletion corresponding to mature CagN (C); CagN^{KFSR}, mutation in predicted DNA binding patch 2 (D).

25 times higher than that of CagN.

3.6. *Functional assays of CagN with respect to substrate transport through the CagT4SS into human target cells*

We hypothesized that CagN, as it binds dsDNA, may contribute to the presumed DNA transport capacities through the CagT4SS. One of the functional assays for CagT4SS is the activation of human epithelial host cells by live, adherent *H. pylori* to produce proinflammatory cytokines such as IL-8 (Censini et al., 1996; Lin et al., 2020; Stein et al., 2017). *H. pylori* also has been shown to, *cag*PAI-dependently, activate human cell TLR9, presumably by translocating DNA through the T4SS (Lin et al., 2020; Varga et al., 2016), but the mechanism has not been uncovered. As reported before, *cagN* mutants have no significantly different phenotype when tested for IL-8 secretion after short-term bacterial co-incubation up to 4 h on gastric epithelial AGS cells (Bourzac et al., 2006; Bats, Coombs, Josenhans, own unpublished data), and *cagN* mutant had no phenotype in a specific set-up in AGS cells for CagA translocation (Fischer et al., 2001). We have recently developed CRISPR-Cas9 knock-out cells of the human gastric AGS cell line and of HEK293-T cells (Stein et al., 2017), deficient in the adapter protein TRAF-interacting protein with a forkhead-associated (FHA) domain (TIFA) (AGS-TIFA$^{k/o}$), that do not respond to bacterial/*H. pylori* heptose metabolites which act as strong MAMPs/PAMPs via early-onset Alpha kinase 1(ALPK1)/TIFA activation (Pfannkuch et al., 2019; Stein et al., 2017; Garcia-Weber et al., 2023). Medium-duration co-incubation of cells with bacteria (20 h to 24 h) was previously reported to trigger cellular responses in AGS cells by *H. pylori* to bacterial nucleotide

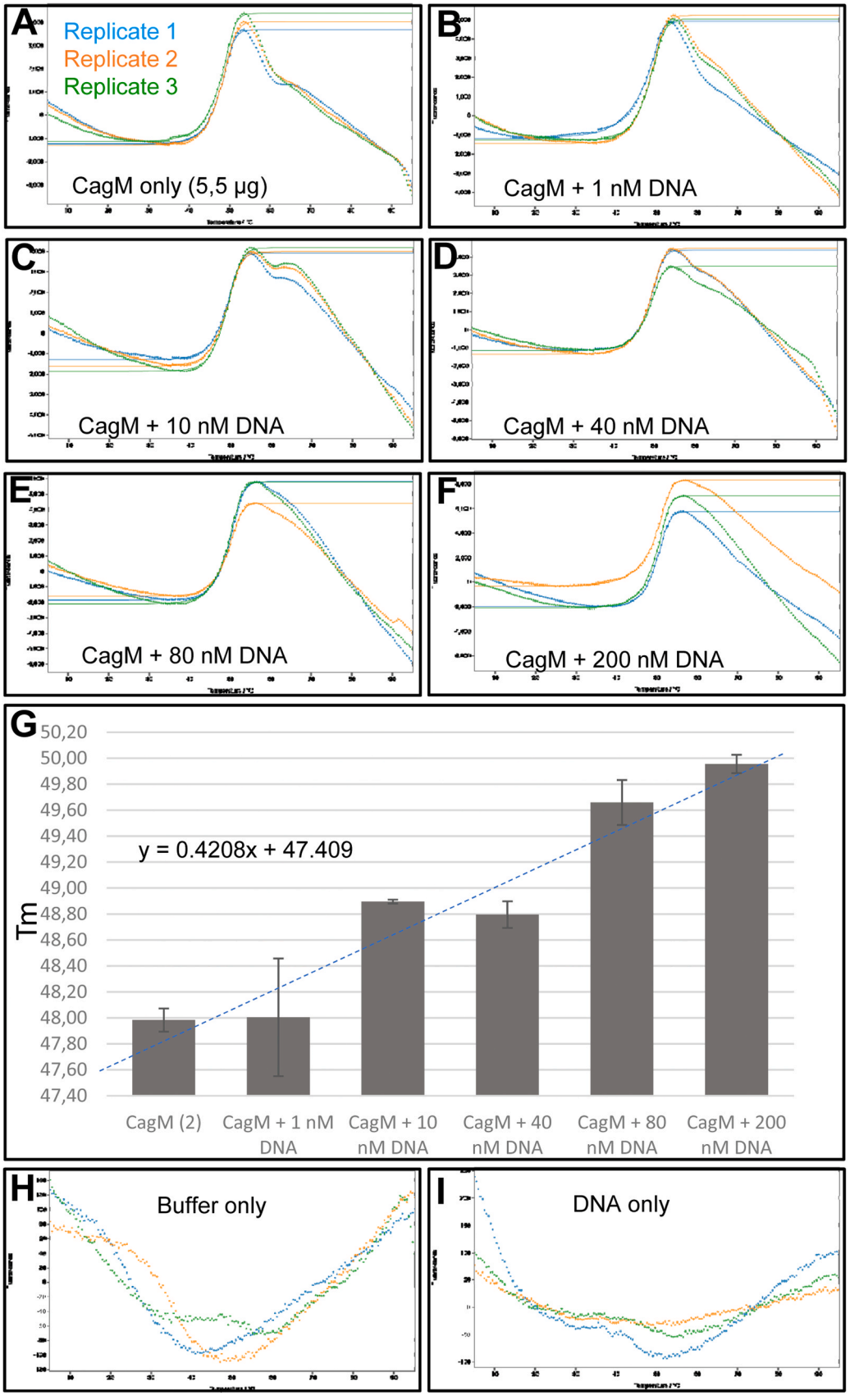

(caption on next page)

Fig. 4. Interaction between CagM and dsDNA verified by TSA. 6 μg CagM^{WT} were either tested alone (A) or coincubated with variable amounts of DNA fragment GC^{39} (A) to F)) in TSA assays. Three representative measurements are displayed for each condition. G) The absolute T_m values (mean) from all triplicate measurements are displayed for the co-incubation samples in a bar graph. A concentration-dependent T_m increase of CagM was detectable after co-incubation with DNA. Linear regression is inserted as a blue dashed line (equation included in figure panel). Obtained relative fluorescence units (RFU) values under conditions without CagM and DNA (H) or without CagM (I) were at least one magnitude lower and negligible. All conditions were measured in triplicates. Colored displays and fits were generated with JTSA (https://github.com/paulsbond/jtsa). A table of numerical TSA results is displayed as Table S5.

oligomerization domain 1 (NOD1) intracellular pattern recognition receptor ligands (muropeptides) (Gall et al., 2017) or DNA (Varga et al., 2016). When we tested the AGS TIFA$^{k/o}$ cells with *H. pylori* (strain N6) wild type, an isogenic mutant in *cagN* (Bats et al., 2018) a reproducible significant phenotype of loss of IL-8 production after medium-term (20 h) co-incubation of the cell line with live bacteria was demonstrated for the isogenic *cagN* mutant (Fig. 5 A). The wild type activation phenotype was recovered in an isogenic *H. pylori* strain complemented in trans by wild type full-length CagN expressed under the control of the *cagMN* operon promoter in the *rdxA* gene (Bats et al., 2018) (Fig. 5 A). Interestingly, a complementation variant with a C-terminally truncated CagN$^{\Delta C90}$ (same promoter construct), which binds less well to CagM (Bats et al., 2018) and to DNA, did not complement the heptose-independent cell activation phenotype (Fig. 5 A). While ADP-heptose, which was used as a control coincubation condition (Fig. S6, (Stein et al., 2017)), expectedly did no longer activate those knock-out cells, we found significant activation of AGS-TIFA$^{k/o}$ cells both with NOD1 ligand ieDAP (Viala et al., 2004) and with ODN2006, a double-stranded oligonucleotide which is a proxy ligand for GCGC-motif-containing human TLR9-agonistic dsDNA (Bauer et al., 2001) (Fig. S6; Fig. 5 A). *E. coli* ultrapure lipopolysaccharide (LPS, TLR4 agonist) or lipopeptide PAMCysS4K (TLR2 agonist) did not activate the cells in the same setup (data not shown). HEK-luciferase NF-κB reporter cells, despite the fact that they display ADP-heptose-dependent activation (Stein et al., 2017), also showed a similar phenotype of significantly reduced NF-κB activation with the *cagN* mutant in comparison to the wild type co-incubated cells (Fig. 5 B).

4. Discussion

In this study, we sought to discover yet unknown properties and functional aspects of the non-canonical and species-specific *H. pylori* CagT4SS protein CagN and its partner protein CagM, which has been shown to be a component of the CagT4SS OMCC (Sheedlo et al., 2022). Previous work investigating a global collection of *cag*PAI-positive strains has established the invariable presence of the *H. pylori*-specific *cagM* and *cagN* genes, which are always organized together in an operon, in the intact *cag*PAIs (Olbermann et al., 2010). While CagM is present in the outer membrane core complex (OMCC) of the T4SS (Sheedlo et al., 2022; Hu et al., 2019) and may guide Cag substrate proteins, such as CagN and others, towards the outer rim of the secretion apparatus, CagN is membrane and surface-localized in the bacteria (Bats et al., 2018). Accordingly, in our previous study comparing global strain diversity of genes within the *cag*PAI, *cagN*/CagN shows considerable non-synonymous between-strain variation (Olbermann et al., 2010), pointing to strong in-vivo selection mechanisms, possibly associated with surface exposure, while *cagM*/CagM is rather highly conserved. We previously determined that CagM binds CagN, with an affinity in the nanomolar range (Bats et al., 2018), with a reduction of binding observed when CagN was C-terminally truncated at its natural cleavage site. This may indicate that CagN is transiently bound to CagM during bacterial membrane transport and can then detach to reach the bacterial surface. Since CagN has no detectable homologs in other bacteria nor in non-bacterial organisms, it was not possible, even with recently introduced improved AlphaFold (versions 2 and 3; (Abramson et al., 2024)) modeling, to derive a protein structure with sufficiently high reliability scores that can possibly aid to design tailored experiments in the quest to elucidate a function. Nevertheless, we were able to use available sequence information to derive potential functionalities of the poorly characterized CagT4SS proteins CagN and its co-expressed tandem partner CagM. CagM has been found before by Cryo-EM to be firmly located as a multimer in a ring structure in the OMCC of the CagT4SS (Sheedlo et al., 2020; Roberts et al., 2024). Presently, the localization findings and prior published functional characterization results (Bats et al., 2018; Fischer et al., 2001; Moese et al., 2001; Sheedlo et al., 2020) point to an essential function of CagM in the export of proteins and other possible substrates of the CagT4SS (Bats et al., 2018). CagM mutants have been found in several previous studies to be completely null in all known functionalities of the CagT4SS, namely CagA translocation and proinflammatory cell activation (Fischer et al., 2001; Moese et al., 2001). Moreover, CagM-deficient mutants have a strong impairment in stabilizing Cag outer proteins, such as CagN and possibly others such as CagL, CagH, CagI (Bats et al., 2018; Fischer et al., 2001). The assembly of the membrane complex of the CagT4SS is hindered when CagM is absent (Frick-Cheng et al., 2016; Hu et al., 2019; Sheedlo et al., 2022). Therefore, it is indeed challenging to study a possible function of CagM in the T4SS transport process in a well-isolated manner in the bacterial context. Due to its orphan nature and the absence of structural information and homologs, the functional characterization of CagN is likewise difficult.

Our present experimental characterization of the purified CagM and CagN proteins in EMSA, SPR and TSA assays show that they both can bind dsDNA. CagN on its own bound dsDNA less well than CagM on its own. We also detected cleavage of dsDNA fragments by both CagN and CagM in the presence of DNA, yielding different cleavage patterns, suggesting that both can act as endonucleases. CagN mutants CagN$^{\Delta C90}$ (truncated) and CagN^{KFSR} site-directed mutant, which replaces four amino acids at the natural cleavage site with alanines, bound DNA less well than CagN wild type and also showed a lower nuclease activity on DNA. Complementary in-silico analysis using Alphafold 3 Multimer (Abramson et al., 2024) structural predictions supported the potential of DNA binding for both proteins, but only in the presence of Mg^{2+} and ATP. Under those in silico conditions, CagN was predicted to exclusively bind to dsDNA as a dimer. This is not completely consistent with but also not contradictory to our previous results which showed that isolated purified CagN, in the absence of DNA, ATP and Mg^{2+}, mostly behaved as a monomer in solution (Bats et al., 2018). The very good binding capacity of CagM to dsDNA lends more credibility to the hypothesis that it may not only help transport proteins to the outer rim of the CagT4SS but also possibly other substrates, such as DNA. We speculate that, for this activity, CagM may cooperate with the co-expressed protein CagN which is encoded downstream of CagM in the same operon. The dsDNA-binding of both proteins seemed to be rather non-specific, since the proteins bound to several different in vitro-generated dsDNA fragments of different sequence and GC content similarly well. This is not implausible, as a similar scenario has also been described for *E. coli* conjugative system proteins TraD and TraE (VirB6 and VirB8 orthologs) in a recent study with no selectivity of binding to specific DNA motifs or segments detected (Jemouai et al., 2025). CagM and CagN, according to our AlphaFold predictions, are anticipated to bind DNA mostly by patches of positively charged amino acids. CagM seems to harbor, as prospective ATP-binding motifs, Walker B- and C-like motifs, however ATP binding was difficult to detect experimentally, although AlphaFold 3 modelling suggested ATP binding for both CagM and CagN (one molecule ATP for each protein subunit). As one hindrance to reliably detect ATP binding, we suspected ATP degradation. Indeed, we obtained

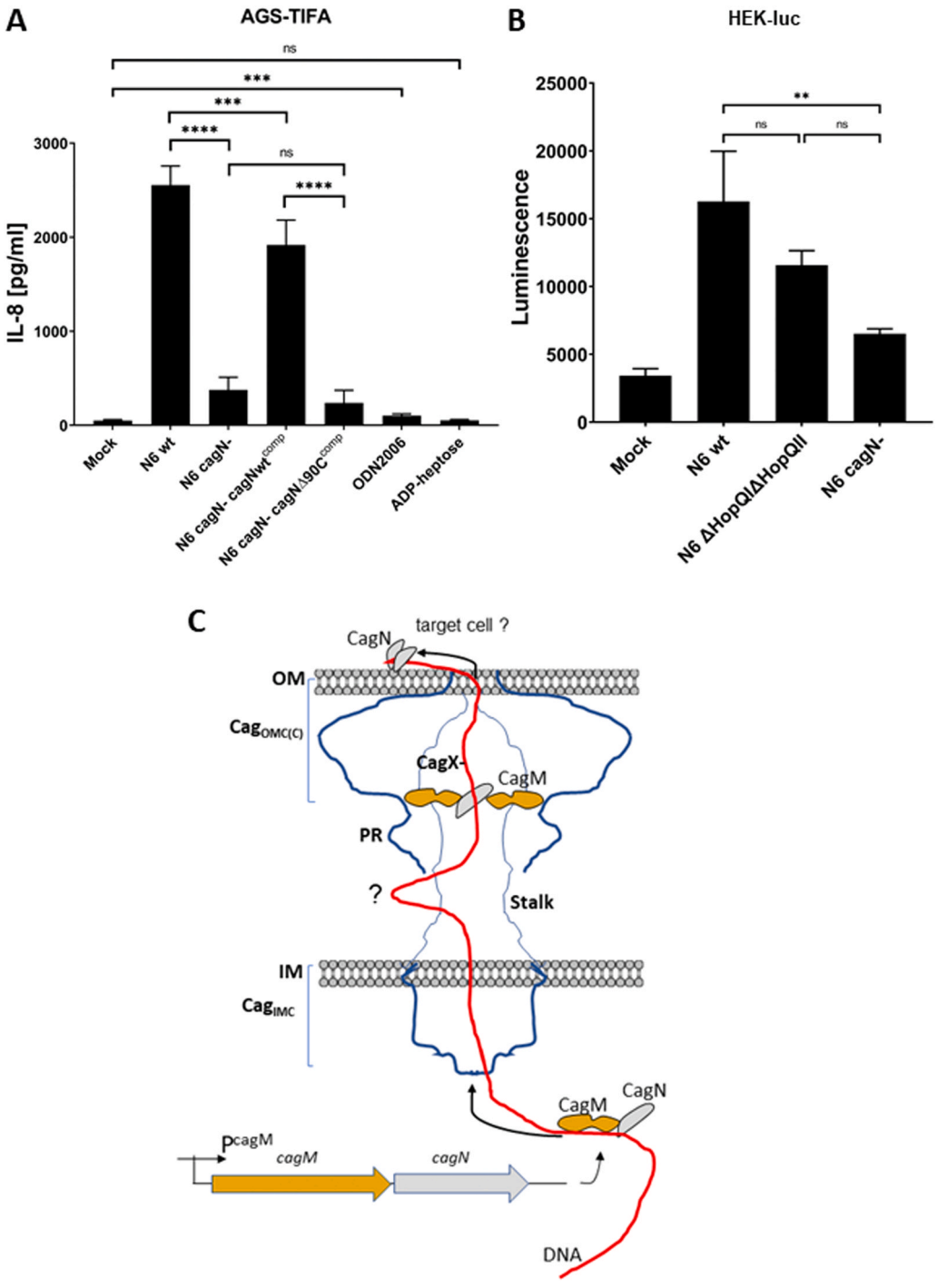

(caption on next page)

Fig. 5. AGS-TIFA k/o cells and HEK-luc reporter cells show CagT4SS-dependent reduction of activation with *H. pylori cagN* mutants which was reconstituted by complementation with full-length CagN; simplified scheme of proposed CagM and CagN functionalities in T4SS. A) AGS-TIFA knock-out cells, which do not show pro-inflammatory activation by ADP-heptose translocated by the *H. pylori* T4SS, were tested for alternative transport and activation functions by the T4SS. Cells in 24-well plates (1×10^5 cells/well) were incubated with *H. pylori* (strain N6) wild type (N6 wt), isogenic *cagN* insertion inactivation mutant (cagN-) and complementants (MOI 25) for 20 h, and chemokine IL-8 released into the supernatant was quantitated by ELISA. *cagN* mutant showed a significantly reduced activity of IL-8 release in the supernatant. Complementant expressing full-length CagN in trans (N6 cagN-cagWT^{comp}) restored IL-8 release. Complementant expressing truncated CagN$^{\Delta C90}$ in trans (N6 cagN-cagΔ90C^{comp}) did not restore IL-8 release. ODN2006 double-stranded oligonucleotide control (300 ng/well, human TLR9 ligand) showed a significant activation over mock (see also supplemental Fig. S6), while ADP-heptose control (ALPK1 agonist, 2.5 μM) did not show significant activation in the TIFA$^{k/o}$ cells. Each data point is derived from six independent measurements. B) HEK-luc NF-κB reporter cells seeded in 96-well plates at 5×10^4 per well were incubated with *H. pylori* wild type (N6 wt), isogenic *hopQ* mutants (N6ΔHopQI-HopQII, control condition for loss of activation by the CagT4SS) and isogenic *cagN* mutant (MOI 50) for 3 h, and luciferase activity was quantitated by luciferase assay. *hopQ* and *cagN* mutants had significantly reduced reporter luciferase activation via the T4SS. Luciferase samples were prepared and measured in biological triplicates. Each experiment was performed at least three times on different days, with similar outcomes. Statistical differences were calculated using Student's *t*-test with pairwise comparisons or Two-way ANOVA with Tukey's post-hoc test. $^{**}p < 0.01$; $^{****}p < 0.0001$; ns = non-significant. C) Simplified schematic model of expression and possible functionalities and localization of CagM and CagN and their DNA binding properties in the *H. pylori* CagT4SS. Protein symbol sizes are not to scale. Since we have not obtained novel data on a potential DNA transport process, question marks indicate uncertainties about the transport and path of transport. Shape of CagT4SS is inspired by the Cryo-EM structures published in (Sheedlo et al., 2022; Roberts et al., 2024). Inner shapes/lumen in the T4SS IMC are not shown, to avoid structural inaccuracies. Inner shapes in the OMC designate the T4SS-OMC lumen. *cagM* and *cagN* bicistronic operon with *cagM* promoter (P^{cagM}) leads to the joint expression of interacting proteins CagM and CagN, which subsequently bind to each other and can bind bacterial DNA (red). The complex may pass through the IMC, possibly with the support of inner membrane ATPases, CagE, Cagα and Cagβ in the IMC, which are not structurally depicted here. CagX (VirB9-ortholog) located in the OMCC channel (Sheedlo et al., 2020) has been reported to interact with DNA (Ryan et al., 2023b), indicated by a hyphen towards the threaded DNA, and with CagM (Sheedlo et al., 2020). CagX is not structurally depicted, and other proteins in the OMC with known interactions to CagM (Busler et al., 2006; Sheedlo et al., 2020) are not shown for schematic clarity. CagN has been detected in the periplasm as well (not shown here; Bourzac et al., 2006), which might be relevant for the transport as indicated with a question mark. Smaller CagN protein symbol indicates the naturally cleaved, C-terminally truncated CagN variant. Truncated mature CagN is detectable on the bacterial surface (Bats et al., 2018), and might also be present in the bacterial cytoplasm, membrane and other locations, which is not shown here due to inconclusive evidence. Surface-located CagN may also interact with other proteins (not shown). Cag$_{OMC(C)}$ designates CagT4SS outer membrane (core) complex; Cag$_{IMC}$ designates inner membrane complex; IM = inner membrane; OM = outer membrane; PR = periplasmic ring of T4SS.

evidence that both proteins can degenerate ATP, and CagM was about 25-fold more active in this property.

CagN protein cleavage close to its C-terminal domain (at amino acid S216) has been described before in *H. pylori* (Bats et al., 2018; Bourzac et al., 2006), even independently of the presence of CagM, without attributing any known function so far. We assume the CagN proteolytic site close to the KFSR motif might be essential for the correct protein production, folding and transport process which could explain the rather low amounts of CagN when we mutated the cleavage site in vivo in *H. pylori* (not shown) which rendered further study of the mutant obsolete. We would be very much interested in studying a function of CagN in the absence of CagM or CagM binding, but so far, loss of CagM in the T4SS or deletion of CagM have not only led to major reduction in abundance of Cag surface proteins including CagN (Bats et al., 2018), but also to structural and functional impairment of the whole T4SS apparatus (Fischer et al., 2001; Hu et al., 2019), in particular the outer membrane complex (Roberts et al., 2024). We assume, backed up by our previous *cagM* mutant analyses in *H. pylori* (Bats et al., 2018), that lack of CagM binding by CagN protein will lead to instability of CagN, which may hamper the further independent characterization of CagN. We have observed before lower CagM binding (Bats et al., 2018) for the mutant CagN$^{\Delta C90}$ deleting the CagN C-terminal domain, which now has led to poor complementation in *H. pylori* cell co-incubation. Therefore, developing an experimental scenario which allows independent study of secreted CagN is challenging. There is certainly a functional importance of CagN binding to CagM, such as ensuring the CagN functionality and integrity during and after membrane transport.

One of our major hypotheses inspiring this study was that CagN, as a dedicated outer protein (Bats et al., 2018), may be intimately involved in transport processes of certain substrates by the CagT4SS towards the host cell. The fact that CagN is C-terminally cleaved upon export also led us to speculate that a cleaved soluble portion may accompany transported cargo towards the host cell. This can be studied, for instance, by human target cell activation through transported Microbe-associated Microbial Patterns (MAMPs) (Gall et al., 2017; Varga et al., 2016). Previous to this study, however, using the frequently used in-vitro assays of co-incubation of gastric epithelial cells (AGS) with live bacteria, *H. pylori* isogenic *cagN* mutants of various wild type isolates initially did not have a reproducible phenotype upon short-time co-incubation with wild type gastric epithelial cell lines, neither in the production of cytokine (IL-8) nor in the translocation of CagA (Bourzac et al., 2006; and own unpublished work). In the first systematic CagT4SS mutagenesis study, Fischer at al. (Fischer et al., 2001) reported an intermediate phenotype of an independently generated *cagN* mutant (not complemented), which had a deficiency in CagA translocation and IL-8 induction that may have been due to a slight polar effect. However, in the present study, using a recently generated gastric epithelial cell line in which heptose-dependent signaling has been eliminated by CRISPR k/o of the cellular signaling adaptor TIFA (Milivojevic et al., 2017; Stein et al., 2017; Garcia-Weber and Arrieumerlou, 2021) (AGS-TIFA$^{k/o}$), we indeed found a reproducible phenotype in that the *cagN* mutants consistently elicited a significantly lower IL-8 induction than the wild type upon co-incubation of the cells with live bacteria for 20 h. The medium time frame of co-incubation in those experiments emphasizes later transportation events through the CagT4SS, such as was previously observed for the translocation of NOD1 ligands (iE-DAP) (Gall et al., 2017) and TLR9 ligands (dsDNA) (Varga et al., 2016). The activation-deficient phenotype of *cagN* mutants specifically in AGS-TIFA$^{k/o}$ cells was significantly recovered by complementing full-length *cagN* in the chromosomal *H. pylori rdxA* locus. These results together with its ability to bind dsDNA, strengthen the notion that CagN can be involved in the translocation of proinflammatory pattern recognition receptor (PRR) ligands (possibly including dsDNA that acts via TLR9, and may also include NOD1 ligands) through the T4SS. Work by others has lent credibility to the concept that the Cag T4SS transports DNA (Varga et al., 2016; Ryan et al., 2023b), and that other proteins of the central T4 secretion complex that we did not study here (such as VirB2-, VirB6-, VirB8-, VirB9(CagX)- and VirB11-orthologs) in various T4SSs indeed can transport and bind DNA (Cascales and Christie, 2004; Whitaker et al., 2015; Fercher, et al., 2016; Ryan et al., 2023b; Maffo-Woulefack et al., 2025; Jemouai et al., 2025; Breidenstein et al., 2025). Those data further support the results of our current molecular and functional study that several different CagT4SS proteins, including now CagM and CagN, might be involved in such functionalities.

Current limitations of our study are that so far that we did not clearly identify the presumed DNA binding region(s) in CagN (or CagM), for instance by site-directed mutagenesis, which might be due to the target region being a complex combination of separate binding patches in the

folded protein rather than a single linear segment. According to our present in-vitro EMSA binding results, the C-terminal domain of CagN might contribute to dsDNA binding as well as the KFSR motif, which is close to the natural CagN cleavage site (Bourzac et al., 2006). Complementing with full-length CagN but not CagN$^{\Delta C90}$ reconstituted the pro-inflammatory T4SS function of *H. pylori cagN* mutants in TIFA knock-out cells. Deleting longer segments of CagN in the mature protein, after deleting its naturally cleaved 90 aa C-terminal domain, is likely to result in conformational changes of the protein and may therefore not deliver conclusive results, and this approach was therefore not performed here. However, additional fine-grained scanning mutagenesis and deletion of smaller patches in CagN (and CagM) could be pursued in the future to clarify the binding properties and functions. We obtained evidence that CagN loss mediated impairment of transport capacities through the CagT4SS, reducing heptose-independent pro-inflammatory activation of human cells. However, the role of DNA in the cell activation phenotype, or the direct contribution of CagN to transport of DNA or other substrates, for instance NOD1 ligands, through the T4SS was neither confirmed nor refuted under those test conditions up to now, since the testing of transport capacities and substrate binding in vivo is challenging. We cannot exclude so far that CagM and CagN DNA binding executes a function exclusively in the bacterial cytoplasm. We also did not test single-stranded DNA in comparison with dsDNA. However, since dsDNA-binding pattern recognition receptor TLR9 was activated by *H. pylori* CagT4SS activity (Varga et al., 2016; Tegtmeyer et al., 2022), it is possible to assume that dsDNA is one potential cargo of the CagT4SS, aided by CagN (Fig. 5 C). We will continue to tackle those functionalities and substrate specificities in future studies.

Taken together, we have obtained evidence towards a potential novel function of CagN and CagM, which relates to dsDNA binding, and possibly to DNA transport through the CagT4SS (hypothetical model in Fig. 5 C). More in-depth experiments and characterization will be needed to unequivocally confirm such functionalities.

CRediT authorship contribution statement

Simon H. Bats: Writing – original draft, Investigation, Supervision, Data curation, Visualization, Formal analysis, Writing – review & editing, Methodology, Conceptualization. **Felix Metz:** Writing – review & editing, Investigation, Validation, Data curation, Visualization, Formal analysis, Methodology. **Johanna Beilmann:** Methodology, Visualization, Formal analysis, Writing – review & editing, Investigation, Validation, Data curation. **Christine Josenhans:** Writing – review & editing, Supervision, Investigation, Conceptualization, Visualization, Project administration, Formal analysis, Writing – original draft, Resources, Funding acquisition, Validation, Methodology, Data curation.

Acknowledgments

We thank Bettina Sedlmaier for expert technical assistance. We are grateful to Claire Cargemel, Regina Wehrstedt von Nessen-Lapp, and Jasmin Forster for experimental contributions during their respective internships. We are extremely grateful for continuous discussions with other lab members of the Josenhans and Suerbaum laboratories. Laurent Terradot is gratefully acknowledged for support in protein purification and characterization. Parts of the project were financially supported by grant B6 from the Deutsche Forschungsgemeinschaft within the CRC 900 consortium (project no. 158989968) to CJ, and by Deutsches Zentrum fuer Infektionsforschung (DZIF) project 06.820 to CJ.

Appendix A. Supporting information

Supplementary data associated with this article can be found in the online version at doi:10.1016/j.ijmm.2025.151661.

Data availability

All data that have been used are contained in the article or are available upon request

References

Abramson, J., Adler, J., Dunger, J., Evans, R., Green, T., Pritzel, A., Ronneberger, O., Willmore, L., Ballard, A.J., Bambrick, J., Bodenstein, S.W., Evans, D.A., Hung, C.C., O'Neill, M., Reiman, D., Tunyasuvunakool, K., Wu, Z., Žemgulytė, A., Arvaniti, E., Beattie, C., Bertolli, O., Bridgland, A., Cherepanov, A., Congreve, M., Cowen-Rivers, A.I., Cowie, A., Figurnov, M., Fuchs, F.B., Gladman, H., Jain, R., Khan, Y.A., Low, C.M.R., Perlin, K., Potapenko, A., Savy, P., Singh, S., Stecula, A., Thillaisundaram, A., Tong, C., Yakneen, S., Zhong, E.D., Zielinski, M., Žídek, A., Bapst, V., Kohli, P., Jaderberg, M., Hassabis, D., Jumper, J.M., 2024. Accurate structure prediction of biomolecular interactions with AlphaFold 3. Nature 630, 493–500.

Alm, R.A., Ling, L.S., Moir, D.T., King, B.L., Brown, E.D., Doig, P.C., Smith, D.R., Noonan, B., Guild, B.C., deJonge, B.L., Carmel, G., Tummino, P.J., Caruso, A., Uria-Nickelsen, M., Mills, D.M., Ives, C., Gibson, R., Merberg, D., Mills, S.D., Jiang, Q., Taylor, D.E., Vovis, G.F., Trust, T.J., 1999. Genomic-sequence comparison of two unrelated isolates of the human gastric pathogen *Helicobacter pylori* [published erratum appears in Nature 1999 Feb 25;397(6721):719]. Nature 397, 176–180.

Andrzejewska, J., Lee, S.K., Olbermann, P., Lotzing, N., Katzowitsch, E., Linz, B., Achtman, M., Kado, C.I., Suerbaum, S., Josenhans, C., 2006. Characterization of the pilin ortholog of the *Helicobacter pylori* type IV *cag* pathogenicity apparatus, a surface-associated protein expressed during infection. J. Bacteriol. 188, 5865–5877.

Atmakuri, K., Cascales, E., Christie, P.J., 2004. Energetic components VirD4, VirB11 and VirB4 mediate early DNA transfer reactions required for bacterial type IV secretion. Mol. Microbiol. 54, 1199–1211.

Bats, S.H., Berge, C., Coombs, N., Terradot, L., Josenhans, C., 2018. Biochemical characterization of the *Helicobacter pylori* Cag Type 4 secretion system protein CagN and its interaction partner CagM. Int. J. Med. Microbiol. 308, 425–437.

Bauer, S., Kirschning, C.J., Häcker, H., Redecke, V., Hausmann, S., Akira, S., Wagner, H., Lipford, G.B., 2001. Human TLR9 confers responsiveness to bacterial DNA via species-specific CpG motif recognition. Proc. Natl. Acad. Sci. 98, 9237–9242.

Behrens, W., Schweinitzer, T., Bal, J., Dorsch, M., Bleich, A., Kops, F., Brenneke, B., Didelot, X., Suerbaum, S., Josenhans, C., 2013. Role of Energy Sensor TlpD of *Helicobacter pylori* in Gerbil Colonization and Genome analyses after adaptation in the Gerbil. Infect. Immun. 81, 3534–3551.

Bernhofer, M., Dallago, C., Karl, T., Satagopam, V., Heinzinger, M., Littmann, M., Olenyi, T., Qiu, J., Schütze, K., Yachdav, G., Ashkenazy, H., Ben-Tal, N., Bromberg, Y., Goldberg, T., Kajan, L., O'Donoghue, S., Sander, C., Schafferhans, A., Schlessinger, A., Vriend, G., Mirdita, M., Gawron, P., Gu, W., Jarosz, Y., Trefois, C., Steinegger, M., Schneider, R., Rost, B., 2021. PredictProtein - predicting protein structure and function for 29 years. Nucleic Acids Res. 49. W535-w540.

Bourzac, K.M., Satkamp, L.A., Guillemin, K., 2006. The *Helicobacter pylori cag* pathogenicity island protein CagN is a bacterial membrane-associated protein that is processed at its C terminus. Infect. Immun. 74, 2537–2543.

Breidenstein, A., Svedberg, D., Ter Beek, J., Berntsson, R.P., 2025. Advances in protein structure prediction highlight unexpected commonalities between gram-positive and gram-negative conjugative T4SSs. J. Mol. Biol. 437, 168924.

Burkovics, P., Hajdú, I., Szukacsov, V., Unk, I., Haracska, L., 2009. Role of PCNA-dependent stimulation of 3′-phosphodiesterase and 3′-5′ exonuclease activities of human Ape2 in repair of oxidative DNA damage. Nucleic Acids Res. 37, 4247–4255.

Busler, V.J., Torres, V.J., McClain, M.S., Tirado, O., Friedman, D.B., Cover, T.L., 2006. Protein-protein interactions among *Helicobacter pylori cag* proteins. J. Bacteriol. 188 (2006), 4787–4800.

Cascales, E., Christie, P.J., 2004. Definition of a bacterial type IV secretion pathway for a DNA substrate. Science 304, 1170–1173.

Censini, S., Lange, C., Xiang, Z., Crabtree, J.E., Ghiara, P., Borodovsky, M., Rappuoli, R., Covacci, A., 1996. *cag*, a pathogenicity island of *Helicobacter pylori*, encodes type I-specific and disease-associated virulence factors. Proc. Natl. Acad. Sci. 93, 14648–14653.

Chen, R., Liliental, J.E., Kowalski, P.E., Lu, Q., Cohen, S.N., 2011. Regulation of transcription of hypoxia-inducible factor-1α (HIF-1α) by heat shock factors HSF2 and HSF4. Oncogene 30, 2570–2580.

Christie, P.J., 1997. *Agrobacterium tumefaciens* T-complex transport apparatus: a paradigm for a new family of multifunctional transporters in eubacteria. J. Bacteriol. 179, 3085–3094.

Costa, T.R.D., Harb, L., Khara, P., Zeng, L., Hu, B., Christie, P.J., 2021. Type IV secretion systems: Advances in structure, function, and activation. Mol. Microbiol. 115, 436–452.

Fercher, C., Probst, I., Kohler, V., Goessweiner-Mohr, N., Arends, K., Grohmann, E., Zangger, K., Meyer, N.H., Keller, W., 2016. VirB8-like protein TraH is crucial for DNA transfer in *Enterococcus faecalis*. Sci. Rep. 6, 24643.

Fischer, W., Püls, J., Buhrdorf, R., Gebert, B., Odenbreit, S., Haas, R., 2001. Systematic mutagenesis of the *Helicobacter pylori cag* pathogenicity island: essential genes for CagA translocation in host cells and induction of interleukin-8. Mol. Microbiol. 42, 1337–1348.

Fischer, W., Tegtmeyer, N., Stingl, K., Backert, S., 2020. Four chromosomal type IV secretion systems in *Helicobacter pylori*: composition, structure and function. Front. Microbiol. 11, 1592.

Frick-Cheng, A.E., Pyburn, T.M., Voss, B.J., McDonald, W.H., Ohi, M.D., Cover, T.L., 2016. Molecular and structural analysis of the *Helicobacter pylori cag* Type IV secretion system core complex. mBio 7, e02001–e02015.
Gall, A., Gaudet, R.G., Gray-Owen, S.D., Salama, N.R., 2017. TIFA signaling in gastric epithelial cells initiates the cag type 4 secretion system-dependent innate immune response to *Helicobacter pylori* infection. mBio 8, e01168-17.
Garcia-Weber, D., Arrieumerlou, C., 2021. ADP-heptose: a bacterial PAMP detected by the host sensor ALPK1. Cell Mol. Life Sci. 78, 17–29.
Garcia-Weber, D., Dangeard, A.S., Teixeira, V., Hauke, M., Carreaux, A., Josenhans, C., Arrieumerlou, C., 2023. In vitro kinase assay reveals ADP-heptose-dependent ALPK1 autophosphorylation and altered kinase activity of disease-associated ALPK1 mutants. Sci. Rep. 13, 6278.
Gomez-Valero, L., Chiner-Oms, A., Comas, I., Buchrieser, C., 2019. Evolutionary dissection of the Dot/Icm system based on comparative genomics of 58 *Legionella* Species. Genome Biol. Evol. 11, 2619–2632.
Guillemin, K., Salama, N.R., Tompkins, L.S., Falkow, S., 2002. Cag pathogenicity island-specific responses of gastric epithelial cells to *Helicobacter pylori* infection. Proc. Natl. Acad. Sci. U. S. A 99, 15136–15141.
Hauke, M., Metz, F., Rapp, J., Faass, L., Bats, S.H., Radziej, S., Link, H., Eisenreich, W., Josenhans, C., 2023. *Helicobacter pylori* modulates heptose metabolite biosynthesis and heptose-dependent innate immune host cell activation by multiple mechanisms. Microbiol Spectr., e0313222
Hellman, L.M., Fried, M.G., 2007. Electrophoretic mobility shift assay (EMSA) for detecting protein-nucleic acid interactions. Nat. Protoc. 2, 1849–1861.
Heuermann, D., Haas, R., 1998. A stable shuttle vector system for efficient genetic complementation of *Helicobacter pylori* strains by transformation and conjugation. Mol. Gen. Genet 257, 519–528.
Hilbi, H., Nagai, H., Kubori, T., Roy, C.R., 2017. Subversion of host membrane dynamics by the *Legionella* Dot/Icm type IV secretion system. Curr. Top. Microbiol. Immunol. 413, 221–242.
Hu, B., Khara, P., Song, L., Lin, A.S., Frick-Cheng, A.E., Harvey, M.L., Cover, T.L., Christie, P.J., 2019a. *In situ* molecular architecture of the *Helicobacter pylori* Cag type IV secretion system. mBio 10. https://doi.org/10.1128/mbio.00849-00819.
Jemouai, Z., Sverzhinsky, A., Sygusch, J., Pascal, J., Baron, C., 2025. Inner membrane components of the plasmid pKM101 type IV secretion system TraE and TraD are DNA-binding proteins. Sci. Rep. 15, 7530.
Kranz, J.K., Schalk-Hihi, C., 2011. Protein thermal shifts to identify low molecular weight fragments. Methods Enzym. 493, 277–298.
Kumar, A., Shukla, S., Mandal, A., Shukla, S., Ambudkar, S.V., Prasad, R., 2010. Divergent signature motifs of nucleotide binding domains of ABC multidrug transporter, CaCdr1p of pathogenic *Candida albicans*, are functionally asymmetric and noninterchangeable. Biochim. Biophys. Acta 1798, 1757–1766.
Labigne-Roussel, A., Courcoux, P., Tompkins, L., 1988. Gene disruption and replacement as a feasible approach for mutagenesis of *Campylobacter jejuni*. J. Bacteriol. 170, 1704–1708.
Lee, P.H., Huang, X.X., Teh, B.T., Ng, L.M., 2019. TSA-CRAFT: a free software for automatic and robust thermal shift assay data analysis. SLAS Discov. Adv. life Sci. R. D. 24, 606–612.
Li, Y.G., Christie, P.J., 2018. The *Agrobacterium* VirB/VirD4 T4SS: mechanism and architecture defined through in vivo mutagenesis and chimeric systems. Curr. Top. Microbiol. Immunol. 418, 233–260 e00790-19.
Lin, A.S., Dooyema, S.D.R., Frick-Cheng, A.E., Harvey, M.L., Suarez, G., Loh, J.T., McDonald, W.H., McClain, M.S., Peek Jr., R.M., Cover, T.L., 2020. Bacterial energetic requirements for *Helicobacter pylori* Cag Type IV secretion system-dependent alterations in gastric epithelial cells. Infect. Immun. 88.
Maffo-Woulefack, R., Ali, A.M., Laroussi, H., Cappèle, J., Romero-Saavedra, F., Ramia, N., Robert, E., Mathiot, S., Soler, N., Roussel, Y., Fronzes, R., Huebner, J., Didierjean, C., Favier, F., Leblond-Bourget, N., Douzi, B., 2025. Elucidating assembly and function of VirB8 cell wall subunits refines the DNA translocation model in Gram-positive T4SSs. Sci. Adv. 11, eadq5975.
Meng, E.C., Goddard, T.D., Pettersen, E.F., Couch, G.S., Pearson, Z.J., Morris, J.H., Ferrin, T.E., 2023. UCSF ChimeraX: tools for structure building and analysis. Protein Sci. 32, e4792.
Milivojevic, M., Dangeard, A.S., Kasper, C.A., Tschon, T., Emmenlauer, M., Pique, C., Schnupf, P., Guignot, J., Arrieumerlou, C., 2017. ALPK1 controls TIFA/TRAF6-dependent innate immunity against heptose-1,7-bisphosphate of gram-negative bacteria. PLoS Pathog. 13, e1006224.
Moese, S., Selbach, M., Zimny-Arndt, U., Jungblut, P.R., Meyer, T.F., Backert, S., 2001. Identification of a tyrosine-phosphorylated 35 kDa carboxy-terminal fragment (p35CagA) of the *Helicobacter pylori* CagA protein in phagocytic cells: processing or breakage? Proteomics 1, 618–629.
Odenbreit, S., Püls, J., Sedlmaier, B., Gerland, E., Fischer, W., Haas, R., 2000. Translocation of *Helicobacter pylori* CagA into gastric epithelial cells by type IV secretion. Science 287, 1497–1500.
Olbermann, P., Josenhans, C., Moodley, Y., Uhr, M., Stamer, C., Vauterin, M., Suerbaum, S., Achtman, M., Linz, B., 2010. A global overview of the genetic and functional diversity in the *Helicobacter pylori cag* pathogenicity island. PLoS. Genet 6, e1001069.
Peña, A., Matilla, I., Martín-Benito, J., Valpuesta, J.M., Carrascosa, J.L., de la Cruz, F., Cabezón, E., Arechaga, I., 2012. The hexameric structure of a conjugative VirB4 protein ATPase provides new insights for a functional and phylogenetic relationship with DNA translocases. J. Biol. Chem. 287, 39925–39932.
Pfannkuch, L., Hurwitz, R., Traulsen, J., Sigulla, J., Poeschke, M., Matzner, L., Kosma, P., Schmid, M., Meyer, T.F., 2019. ADP heptose, a novel pathogen-associated molecular pattern identified in *Helicobacter pylori*. FASEB J. 33, 9087–9099.
Qin, L., Zheng, J., Grant, C.E., Jia, Z., Cole, S.P., Deeley, R.G., 2008. Residues responsible for the asymmetric function of the nucleotide binding domains of multidrug resistance protein 1. Biochemistry 47, 13952–13965.
Roberts, J.R., Tran, S.C., Frick-Cheng, A.E., Bryant, K.N., Okoye, C.D., McDonald, W.H., Cover, T.L., Ohi, M.D., 2024. Subdomains of the *Helicobacter pylori* Cag T4SS outer membrane core complex exhibit structural independence. Life Sci. Alliance 7, e202302560.
Ryan, M.E., Damke, P.P., Shaffer, C.L., 2023a. DNA transport through the dynamic type IV secretion system. Infect. Immun. 91, e0043622 (a).
Ryan, M.E., Damke, P.P., Bryant, C., Sheedlo, M.J., Shaffer, C.L., 2023b. Architectural asymmetry enables DNA transport through the *Helicobacter pylori cag* type IV secretion system. bioRxiv [Preprint]. Jul 26:2023.07.25.550604.
Schulz, M.N., Landström, J., Hubbard, R.E., 2013. MTSA–a Matlab program to fit thermal shift data. Anal. Biochem. 433, 43–47.
Sheedlo, M.J., Chung, J.M., Sawhney, N., Durie, C.L., Cover, T.L., Ohi, M.D., Lacy, D.B., 2020a. Cryo-EM reveals species-specific components within the *Helicobacter pylori* Cag type IV secretion system core complex. eLife 9, e59495.
Sheedlo, M.J., Ohi, M.D., Lacy, D.B., Cover, T.L., 2022. Molecular architecture of bacterial type IV secretion systems. PLOS Pathog. 18, e1010720.
Stein, S.C., Faber, E., Bats, S.H., Murillo, T., Speidel, Y., Coombs, N., Josenhans, C., 2017. *Helicobacter pylori* modulates host cell responses by CagT4SS-dependent translocation of an intermediate metabolite of LPS inner core heptose biosynthesis. PLoS Pathog. 13, e1006514.
Stein, M., Rappuoli, R., Covacci, A., 2000. Tyrosine phosphorylation of the *Helicobacter pylori* CagA antigen after *cag*-driven host cell translocation. Proc. Natl. Acad. Sci. 97, 1263–1268.
Tan, S., Noto, J.M., Romero-Gallo, J., Peek Jr., R.M., Amieva, M.R., 2011. *Helicobacter pylori* perturbs iron trafficking in the epithelium to grow on the cell surface. PLoS. Pathog. 7, e1002050.
Tegtmeyer, N., Linz, B., Yamaoka, Y., Backert, S., 2022. Unique TLR9 Activation by *Helicobacter pylori* Depends on the *cag* T4SS, But Not on VirD2 Relaxases or VirD4 Coupling Proteins. Curr. Microbiol. 79, 121.
Varga, M.G., Shaffer, C.L., Sierra, J.C., Suarez, G., Piazuelo, M.B., Whitaker, M.E., Romero-Gallo, J., Krishna, U.S., Delgado, A., Gomez, M.A., Good, J.A., Almqvist, F., Skaar, E.P., Correa, P., Wilson, K.T., Hadjifrangiskou, M., Peek, R.M., 2016. Pathogenic *Helicobacter pylori* strains translocate DNA and activate TLR9 via the cancer-associated cag type IV secretion system. Oncogene 35, 6262–6269.
Viala, J., Chaput, C., Boneca, I.G., Cardona, A., Girardin, S.E., Moran, A.P., Athman, R., Memet, S., Huerre, M.R., Coyle, A.J., DiStefano, P.S., Sansonetti, P.J., Labigne, A., Bertin, J., Philpott, D.J., Ferrero, R.L., 2004. Nod1 responds to peptidoglycan delivered by the *Helicobacter pylori cag* pathogenicity island. Nat. Immunol. 5, 1166–1174.
Waksman, G., 2025. Molecular basis of conjugation-mediated DNA transfer by gram-negative bacteria. Curr. Opin. Struct. Biol. 90, 102978.
Walker, J.E., Eberle, A., Gay, N.J., Runswick, M.J., Saraste, M., 1982. Conservation of structure in proton-translocating ATPases of *Escherichia coli* and mitochondria. Biochem Soc. Trans. 10, 203–206.
Whitaker, N., Chen, Y., Jakubowski, S.J., Sarkar, M.K., Li, F., Christie, P.J., 2015. The all-alpha domains of coupling proteins from the *Agrobacterium tumefaciens* VirB/VirD4 *and Enterococcus faecalis* pCF10-Encoded Type IV secretion systems confer specificity to binding of cognate DNA substrates. J. Bacteriol. 197, 2335–2349.
Yu, D.J., Hu, J., Huang, Y., Shen, H.B., Qi, Y., Tang, Z.M., Yang, J.Y., 2013. TargetATPsite: a template-free method for ATP-binding sites prediction with residue evolution image sparse representation and classifier ensemble. J. Comput. Chem. 34, 974–985.
Zimmermann, S., Pfannkuch, L., Al-Zeer, M.A., Bartfeld, S., Koch, M., Liu, J., Rechner, C., Soerensen, M., Sokolova, O., Zamyatina, A., Kosma, P., Maurer, A.P., Glowinski, F., Pleissner, K.P., Schmid, M., Brinkmann, V., Karlas, A., Naumann, M., Rother, M., Machuy, N., Meyer, T.F., 2017. ALPK1- and TIFA-dependent innate immune response triggered by the *Helicobacter pylori* type IV secretion system. Cell Rep. 20, 2384–2395.